

Document downloaded from:

<http://hdl.handle.net/10251/52203>

This paper must be cited as:

Fernández Sáez, J.; Del Río García, A.I.; Molina Puerto, J.; Bonastre Cano, J.A.; Cases Iborra, F.J. (2015). Modified carbon fabric electrodes: preparation and electrochemical behavior toward amaranth electrolysis. *Journal of Applied Electrochemistry*. 45(3):263-272. doi:10.1007/s10800-014-0769-9.



The final publication is available at

<http://dx.doi.org/10.1007/s10800-014-0769-9>

Copyright Springer Verlag (Germany)

Non-modified and platinum/polyaniline-modified carbon fiber fabric electrodes: preparation and electrochemical behavior towards amaranth electroreduction/electrooxidation electrolysis

J. Fernández ^a, A.I. del Río ^a, J. Molina ^{a,b}, J. Bonastre ^a, F. Cases ^{a,*}

^a*Departamento de Ingeniería Textil y Papelera, Escuela Politécnica Superior de Alcoy, Universitat Politècnica de València, Plaza Ferrándiz y Carbonell, s/n, 03801 Alcoy, Spain.*

^b*Department of Textile Engineering, University of Minho, Campus de Azurém, 4800-058 Guimarães, Portugal.*

Abstract

The electrochemical behavior of non-modified, Pt-modified and Pt/polyaniline-modified carbon fiber textile electrodes was studied through a series of electroreduction/electrooxidation electrolyses, performed under potentiostatic conditions, for an amaranth/sulphuric solution in the presence or absence of chloride ion. Both Pt electrodeposition and aniline polymerization were carried out potentiodynamically by cyclic voltammetry (CV). The morphology of the dispersed Pt, PANI, and PANI/Pt coatings on the textile surface was analyzed by scanning electron microscopy (SEM) and stereoscopic imaging. Scanning electrochemical microscopy (SECM) was used to confirm that the electrocatalytic material synthesized on the textile surface, coats and modifies effectively the electroactivity of the carbon fiber fabric.

The amaranth electrolyses were carried out potentiostatically and monitored in terms of specific charge efficiency and electrolysis time. The color removal reached values above 90 % in both electroreduction and electrooxidation processes. The amaranth electroreductions carried out with the non-modified electrode showed better charge efficiency than those with the Pt-modified textile electrode. A significant reduction in electrolysis time for the amaranth electrooxidations was obtained when Pt modified textile electrodes were used. Ultraviolet-visible and Fourier transform infrared spectroscopy with attenuated total reflection (FTIR-ATR) spectra allowed us to distinguish the different electrochemical behavior of the non-modified and Pt/PANI-modified electrodes towards the amaranth electroreduction/electrooxidation.

Keywords: Carbon fabric electrodes; Dispersed platinum; Polyaniline; Amaranth electrolysis

* Corresponding author. Tel.: +34 96 652 84 12; fax: +34 96 652 84 38.

E-mail address: fjcases@txp.upv.es (F. Cases).

1 Introduction

Carbon materials are of special interest due to their properties, such as size, porosity, chemical stability, corrosion resistance, good thermal resistance and electrical conductivity [1-3]. Textile materials as substrates for electrodes offer a large number of geometrical possibilities for their design, a high effective area per geometric unit and, the manufacturing processes are technically and economically more favorable than those for metal substrates. Conducting polymers are useful supports for the

immobilization of dispersed noble metal catalysts and due to the relatively high electrical conductivity of some polymers it is possible to transfer electrons through polymer chains, between the electrodes and dispersed metal particles, where the electrocatalytic reaction occurs [4]. The electrochemical deposition of Pt particles on carbon supports and conductive polymers for the electrooxidation of small organic molecules (CH_3OH , HCHO and HCOOH) has been extensively investigated [5-11].

The research carried out in the present work is included within the context of applied electrochemistry for the treatment of dyeing wastewater from textile industries polluted with azo dyes. Two working electrodes were developed from the carbon fiber fabric: one-dimensional (WE1D) and two-dimensional (WE2D) electrodes. WE1D were used to define the synthesis conditions for Pt electrodeposition and aniline electropolymerization since WE2D electrodes did not provide proper voltammetric information. With respect to the above, SECM has been proved as a useful alternative to CV in determining whether the electrocatalytic material coats and modifies effectively the textile surface.

On this basis, the electroreduction/electrooxidation electrolyses of a much more complex molecule, such as the azo dye amaranth, were studied individually in a separated compartments cell using carbon fiber based textile electrodes in the presence/absence of chloride ion. Amaranth was chosen for this work because it presents the basic structure of other more complex azo dyes such as C.I. Reactive Black 5 or C.I. Reactive Orange 4, which are subjects of study by our research group.

The electrolyses were monitored in terms of percentage of decolorization versus specific charge and time of electrolysis. Samples taken during these processes were analyzed by UV-visible and FTIR-ATR spectroscopies [12]. FTIR-ATR spectra

provided good evidences of the different pathways for the amaranth electrooxidation depending on the kind of electrode and the presence/absence of chloride ion.

2 Materials and methods

2.1 Reagents and chemicals

Amaranth ($C_{20}H_{11}N_2Na_3O_{10}S_3$) was provided by Fluka. Analytical grade sulphuric acid (H_2SO_4), anhydrous potassium sulphate (K_2SO_4) and hexachloroplatinic acid hexahydrate ($H_2PtCl_6 \cdot 6H_2O$) were purchased from Merck. Anhydrous hexaammineruthenium (III) chloride ($Ru(NH_3)_6Cl_3$) 98% was used as received from Acrōs Organics. Aniline was supplied by Merck and was purified by distillation before use. Distillation was performed at reduced pressure in order to avoid thermal degradation of the monomer. After distillation, aniline was stored in the dark at 0-5 °C. When needed, solutions were deoxygenated by bubbling nitrogen gas (N_2 premier X50S). Ultrapure water was obtained from an Elix 3 Millipore-Milli-Q Advantage A10 system with a resistivity near to 18.2 MΩ cm.

2.2 Preparation of electrodes

2.2.1 Textile electrodes

The company Carbongen S.A. (Spain) supplied the hydrophilic activated carbon fabric (ref. HST 1110). In order to discard the presence of impurities on the surface of the fabric, a previous analysis (not included) by FTIR-ATR was carried out. The technical

characteristics of the activated carbon fabric are reported in Table 1. Two carbon textile electrodes with one-dimensional (WE1D) or two-dimensional geometry (WE2D) were made by taking out a yarn or cutting 1 cm x 3 cm strip from the carbon fabric, respectively. In order to ensure a proper electric contact, textile samples were glued to either copper wires or 2 mm diameter copper rods (the tip was flattened to improve the electrical contact) using CircuitWorks[®] conductive epoxy resin by Chemtronics[®]. The resin was hardened in an oven at 90 °C and wrapped with Teflon tape to protect it from the solution.

2.2.2 Glassy carbon electrode

The surface of the glassy carbon electrode (GC) (3 mm diameter) used in the CV experiments, was polished before use with Micropolish II[®] alumina 0.05 µm from Buehler[®]. The GCE was then washed with water and treated in an ultrasonic bath to eliminate the remaining alumina.

2.3 CV

CV measurements with WE1D and GC were performed in a conventional voltammetric cell. Two rods of stainless steel (3.5 mm diameter) were used as counter electrodes (CE). CV experiments with WE2D were carried out in a 250 cc glass beaker equipped with a stainless steel cylindrical mesh (4.5 cm height and 3.5 cm diameter) as CE. The WE2D was placed in the middle of the cylinder and immersed in the solution. Due to the lack of proper voltammetric information when using WE2D, the range of potentials for the electropolymerization of aniline and the electrodispersion of Pt particles had to

be established using the textile electrode WE1D. Thus, the electropolymerization of aniline on WE2D was performed in 0.1 M distilled aniline and 0.5 M H₂SO₄ solution by cycling the potential 5 times between -125 and 1000 mV at 5 mV s⁻¹. Immediately after the synthesis process, the WE2D/PANI surface was washed in a gently stirred 0.5 M H₂SO₄ solution to remove the excess polymer. The electrodispersion of Pt on WE2D and WE2D/PANI was carried out by cycling the potential 20 times between -250 mV and 400 mV in 5 mM H₂PtCl₆·6H₂O and 0.5 M H₂SO₄ solution at a scan rate of 10 mV s⁻¹. All CV measurements were carried out with an Autolab PGSTAT302 potentiostat/galvanostat. The ohmic potential drop was measured and introduced in the Autolab software (GPES).

2.4 SECM

SECM measurements were obtained with a scanning electrochemical microscope from Sensolytics. The three-electrode cell configuration consisted of a 100 μm diameter Pt SECM-tip, a Pt wire as auxiliary electrode and Ag/AgCl (3 M KCl) as reference electrode. The reference electrode was placed in contact with the solution through a Luggin capillary. SECM experiments were carried out in a 0.01 M Ru(NH₃)₆Cl₃ and 0.1 M K₂SO₄ solution with the SECM-tip potential held at -300 mV to reduce the oxidized form of the mediator, Ru(NH₃)₆³⁺, at the diffusion-controlled rate. The pH was adjusted with 0.01 M KOH and 0.01 M H₂SO₄ solutions. Electrode samples of WE2D/PANI and WE2D/PANI-Pt were treated for 1 hour at pH 2.5 and 5.5 and dried in a desiccator. Samples of 5 mm x 5 mm were cut and glued with epoxy resin on glass microscope slides. SECM experiments were performed at open circuit potential (OCP). That is to say, the potential of the substrates was indirectly controlled by the redox mediator

concentration. Oxygen was removed from solutions by bubbling nitrogen and then an inert atmosphere was maintained.

The SECM-tip was moved in z direction and the tip current was recorded. In accordance with SECM theory, the tip current is expressed in terms of normalized current. The normalized current is defined as $I_T = i/i_\infty$ where i_∞ is the diffusion current limit defined as $i_\infty = 4 n F D a C$ where: n is the number of electrons involved in the reaction, F is the Faraday constant, D is the diffusion coefficient, a is the radius of the SECM-tip and C is the concentration of the mediator. The normalized current depends on RG and L . RG is defined as $RG = R_g/a$ where R_g is the radius of the insulating glass surrounding the tip of radius a . L is defined as $L = d/a$ where d is the substrate/SECM-tip separation. According to Sensolytics, the RG of our SECM-tip is $RG \geq 20$.

The experimental approach curves (I_T vs L) were compared with the theoretical positive feedback model. According to Rajendran et al. [13], Pade's approximation gives a simple equation with less relative error for all distances and valid for $RG > 10$. The approximate expression of the steady-state normalized current assuming positive feedback for a glass finite insulator thickness is:

$$I_T = \left(\frac{1 + \frac{1.5647}{L} + \frac{1.31685}{L^2} + \frac{0.4919707}{L^3}}{1 + \frac{1.123}{L} + \frac{0.6263951}{L^2}} \right)$$

2.5 Stereoscopic imaging and SEM characterization

Images of the electrode surfaces were taken with a SteREO microscope Discovery V8 from Zeiss. The microscope captures a number of images with different levels of focus and creates the resultant image.

A Jeol JSM-6300 scanning electron microscope was used to observe the morphology of the samples. SEM samples were coated with Au using a Sputter Coater Bal-Tec SCD 005. SEM analyses were performed using an acceleration voltage of 20 kV.

2.6 Electrolytic processes

The electrolyses were carried out in a divided cell (H shape) with anodic and cathodic compartments separated by means of a cationic membrane (Nafion 117 from DuPont). The different WE2D (1 cm x 1 cm geometric area) were introduced in the compartment filled with 55 ml of 60 mg L⁻¹ amaranth and 0.5 M H₂SO₄ solution. A Pt wire (1 cm² geometric area) was used as CE and introduced in the other compartment with 55 ml of 0.5 M H₂SO₄ solution. Two Ag/AgCl (3 M KCl) were used as reference electrodes. An Autolab PGSTAT302 potentiostat/galvanostat was used to control the potential. The electrolytic processes were analyzed by measuring the percentage of color removal versus the specific charge applied Q (A h L⁻¹) and time of electrolysis t (h). The percentage of decolorization was calculated by measuring the area of the chromatographic peak corresponding to the amaranth molecule as follows:

$$\% = 100 * \frac{(A_0 - A)}{A_0}$$

where A_0 and A are the area values before and after treatment, respectively.

2.7 High performance liquid chromatography (HPLC), UV-visible and FTIR-(ATR)

The area of the amaranth chromatographic peak was calculated from the chromatograms obtained using a system consisting of a Hitachi Elite Lachrom Chromatographic System equipped with a diode array detector. The column was a Lichrospher 100 RP-18C with 5 μm packing. The mobile phase composition was methanol (eluent A)/aqueous buffer solution NaH_2PO_4 - Na_2HPO_4 (eluent B) with $\text{pH}= 6.9$. Separation was accomplished at a flow rate of 1 mL min^{-1} , at 298 K and injection volume of 20 μL . At the beginning of the chromatographic separations, the gradient elution consisted of 15 % methanol-85 % aqueous buffer and it was progressively modified to 30 % methanol-70 % aqueous buffer for 10 min. The UV-visible spectra were recorded with the same equipment but, in this case, the chromatographic column was replaced by a stainless tube provided by the supplier of the equipment. In this procedure, the sample was injected using methanol as solvent and reached the detector without separation of its components.

The FTIR-ATR spectra were recorded with a spectrophotometer FTIR NICOLET 6700 equipped with an ATR device in which the bottom of the surface prism (ZnSe) serves as the cavity for aqueous samples. The subtraction of the background signal (0.5 M H_2SO_4) was required to obtain the spectra of the different samples.

3 Results and discussion

3.1 Coating of electrodes

Cyclic voltammetry was chosen to carry out the coating processes of Pt electrodeposition and aniline electropolymerization. For the Pt coating, the

potentiodynamic method provides surfaces with better catalytic activity compared to other procedures such as potentiostatic synthesis [7]. In the case of the electropolymerization, Niu et al. [14] proved that the polymer synthesized potentiodynamically shows better adherence, optical properties and morphology. Fig. 1a shows the voltammograms obtained during the electrodeposition of Pt particles. Fig. 1b describes the electropolymerization of aniline on WE2D. It can be seen that the characteristic peaks are not observable in these voltammograms due to the high background current. Therefore, a voltammetric study with a textile WE1D was previously performed to establish the potential ranges for the electrodispersion of Pt and the electropolymerization of aniline. Well-defined voltammetric peaks are observed in Fig. 1c. In order to establish the limits of the electroreduction potential range for the electrodeposition of Pt, a first cycle between -300 and 400 mV was performed. On the basis of this result -250 mV was selected as the electroreduction potential limit. Fig. 1d shows the CV of PANI synthesis between -125 mV and 875 mV. Characteristic peaks at around 250 mV, 600 mV and 850 mV corresponding to the leucoemeraldine/emeraldine conversion, redox reaction of degradation products (hydroquinone to quinone) and emeraldine/pernigraniline, were clearly identified according to Huang et al. [11]. The CV of the electrodeposition of Pt on WE2D/PANI is given in Fig. 1e. An increase in the current with the number of cycles was observed. This result indicates an autocatalytic effect of the electroactive materials and an increase in surface area.

3.2 SECM characterization

In section 3.1, it was shown that only with the WE1D electrodes it was possible to obtain a distinctive voltammetric response of the synthesis processes. SECM

characterization is proposed in the present work to analyze whether the amount of Pt or PANI on the surface of the carbon fabric (WE2D) is adequate to change the initial electrochemical properties of the carbon surface. The approach curves recorded on WE2D, WE2D/Pt, WE2D/PANI and WE2D/PANI-Pt at pH = 2.5 are shown in Fig. 2a. As can be seen, positive feedback is obtained ($I_T > 1$) which indicates that the samples are electroactive and capable of reoxidizing the reduced form of the redox mediator. Fig. 2b shows the different electroactivity between WE2D and WE2D/PANI at pH = 5.5. At this pH, the WE2D/PANI surface loses its activity although no negative feedback is observed. This fact indicates that the deactivated polymer is distributed on the carbon fabric shielding the initial electroactivity of the carbon fiber fabric. On the other hand, the approach curves on WE2D/PANI-Pt at pH = 5.5 maintain the increase in normalized current ($I_T > 1$). This indicates that the dispersed Pt particles coat the electropolymerized PANI on the carbon surface, creating a conductive surface at pH = 5.5.

3.3 SEM and stereoscopic images

Fig. 3a shows a stereoscopic image of the WE2D/Pt surface. The carbon fibers appear to be coated homogeneously without discontinuities (uncoated areas) or massive clusters. SEM micrographs show that the coated fibers exhibit a compact distribution of Pt particles. Two different magnifications were selected to appreciate the size and shape of the Pt microparticles. Fig. 3b shows two SEM micrographs of WE2D/PANI surface. PANI polymer shows a fibrous morphology and coats the carbon fibers leaving empty interstices on the carbon fiber. SEM micrographs in Fig. 3c show that Pt particles nucleation occurs on both PANI structures and void spaces of the carbon fiber surface.

3.4 Voltammetric study of amaranth

3.4.1 WE1D and GC electrodes

In section 3.1, the voltammetric experiments were carried out with a textile electrode in the one-dimensional configuration (WE1D). With this geometry it was possible to distinguish the different processes taking place on its surface by CV. As can be seen in Figs. 4a and b for the amaranth solution, this strategy did not provide proper voltammograms in which the amaranth electroreduction/electrooxidation peaks appeared clearly identified. Assuming that the glassy carbon surface (GC) differs from that of the activated carbon, a GC electrode was selected to establish the potential peaks for the amaranth azo dye. Fig. 4c shows the voltammogram with the two characteristic peaks at 0 mV and 900 mV for the amaranth reduction and oxidation, respectively. These potentials were chosen as reference values for the potentiostatic electrolysis carried out with the WE2Ds.

3.5 Electrochemical study

3.5.1 Electroreduction

Fig. 5 shows the curves of % of decolorization for the amaranth electroreduction on WE2D (at 0 mV, -500 mV and -800 mV) and WE2D/Pt (at 0 mV and -100 mV). The evolution of the curves in Fig. 5a indicates that, compared to the electrolysis performed with WE2D at 0 mV, the electrolyses carried out with WE2D at -500 mV and -800 mV show less current efficiency. This result is consistent with the value of the voltammetric

peak for the amaranth electroreduction at 0 mV. The electrolyses carried out with WE2D/Pt electrodes at 0 mV and -100 mV show also less charge efficiency as a consequence of the competitive processes on the Pt surface at 0 mV and -100 mV in acidic medium. In Fig. 5b, the plot % decolorization vs. time of electrolysis shows that the electrolyses carried out at -500 mV and -800 mV present (from 50 %) faster kinetic than in the other electrolyses. This result indicates that higher potentials improve the kinetic of the amaranth electroreduction for WE2D electrode. On the other hand, the presence of Pt does not improve the kinetic of the amaranth electroreduction.

3.5.2 Electrooxidation

The results obtained for the amaranth electrooxidation on WE2D, WE2D/Pt and WE2D/PANI-Pt at 900 mV in the presence/absence of chloride ion are shown in Fig. 6. As can be seen from the curves of the % decolorization vs. specific charge, the electrooxidation electrolyses present a similar percentage of color removal at the end of the treatment for all electrodes. This result differs from that obtained in the electroreduction with WE2D/Pt in which the loss of efficiency continued throughout the entire process. With regard to this, the temporary low efficiency of the electrooxidation on WE2D/Pt and WE2D/PANI-Pt at the beginning of the process was analyzed by performing the amaranth electrooxidation in the presence of 0.3 g L^{-1} chloride ion. This concentration was chosen according to the studies reported by Sala et al. [15]. As can be seen in Fig. 6a, an increase in the color removal efficiency has been observed for WE2D/Pt and WE2D/PANI-Pt electrodes. A possible explanation for this could be based on the transitory electrochemical processes that take place on the platinum surface at 900 mV. According to Priyantha et al. [16], in the absence of chloride ion, the oxide

formation would compete temporarily with the amaranth oxidation at the beginning of the electrolysis until the stabilization of the surface. In the presence of chloride ion, platinum-chloride complexes are formed by the adsorption of chloride species at potentials higher than that required for common platinum oxide formation of 600 mV vs. SCE. The oxidative effect of the chlorinated species on amaranth could be the reason for the specific charge efficiency increase in the $[0, 0.02 \text{ A h L}^{-1}]$ interval. This item will be analyzed in the spectroscopic analysis section. Fig. 6b shows a significant decrease of the electrolysis time for the electrolyses carried out with WE2D/Pt and WE2D/PANI-Pt. This result indicates that the dispersion of Pt on the carbon textile surface involves an improvement in the electrocatalytic properties of the bare carbon WE2D towards the electrooxidation of amaranth.

3.6 Spectroscopic analysis

3.6.1 Electroreduction

The UV-visible spectra of samples taken during the amaranth electroreduction are shown in Fig. 7. In order to simplify the spectra, only the analysis of the samples taken at the end of the electrolysis (after 0.4 A h L^{-1}) are shown. In Fig. 7a, the UV-visible spectra show the complete disappearance of the peak at 520 nm which corresponds to the chromophore group (responsible for the solution color) of the azo dye. The UV region in Fig. 7 seems to have undergone certain modifications but, in essence, maintains the same characteristics for all the electrolyses and electrodes. This result could mean that the species from the electroreductions maintain their aromatic structures responsible for the UV region of the spectrum.

3.6.2 Electrooxidation

The UV-visible spectra of samples taken at the end of the amaranth electrooxidation (after 0.07 A h L^{-1}) are shown in Fig. 8. In Fig. 8a, the spectra obtained for the non-modified WE2D and modified WE2D/Pt, WE2D/PANI-Pt in the absence of chloride ion are shown. The characteristic peak at 520 nm disappears for all the electrodes which means the rupture of the amaranth chromophore group and the consequent decolorization of the amaranth solution. The characteristic peak at 330 nm also disappears. The decrease in the area of the UV region for WE2D/Pt, and particularly for WE2D/PANI-Pt modified textile electrodes is worth highlighting. Fig. 8b shows the UV-visible spectra in the presence of chloride ion. The disappearance of the peak at 520 nm again took place and the peak at 250 nm shows an increase in intensity for both WE2D/Pt and WE2D/PANI-Pt. It is difficult to draw definitive conclusions analyzing the UV region of the spectra. Therefore an analysis by FTIR-ATR was carried out.

3.6.3 FTIR-ATR analysis

Fig. 9 shows the FTIR-ATR obtained for the samples taken at the end of the amaranth electroreduction/electrooxidation. As can be seen in the spectrum for the initial amaranth solution, two characteristic bands ascribed to SO_3 symmetric and asymmetric stretching vibrations and naphthalene rings deformation at 1050 cm^{-1} (I) and 1190 cm^{-1} (II) are identified. There is also a less intense band at around 1625 cm^{-1} (III) that could correspond to the imine group (C=N-) in the tautomeric form of amaranth [12]. The final sample from the electroreduction with better specific charge efficiency (on WE2D

at 0 mV) was analyzed. The first two bands have disappeared from the spectrum. This could be as a result of the SO_3 reductions and the modification of the naphthalene structure. The band at 1625 cm^{-1} appears wider and more intense. This result could be related to the bending of the amine N-H bond resulting from the reduction of the chromophore group.

The spectra for the electrooxidation carried out with WE2D and WE2D/Pt show the same bands than that of the amaranth solution. This result indicates that the species generated during the electrooxidation maintain their aromatic structure relatively intact together with the sulphonic groups. The same analysis in presence of Cl^- for WE2D/Pt shows that bands I and II have disappeared. This result could be understood as being due to the oxidative effect of the chlorinated species on amaranth and would provide evidence of a different pathway for the amaranth electrooxidation in the presence of chloride ion. The spectra for WE2D/PANI-Pt in absence of Cl^- show the disappearance of bands I and II which is consistent with the UV spectra for WE2D/PANI-Pt where a remarkable loss of characteristic peaks and intensity was observed.

4. Conclusions

The carbon fabric showed good electrocatalytic activity in aqueous solution. This fact means that it is a suitable substrate to be coated with electroactive materials such as conductive polymers or dispersed Pt using electrochemical procedures. SECM microscopy has been proven to be an efficient alternative to the classic techniques of electroanalysis especially with samples coated with electroactive materials that do not provide proper voltammetric information such as WE2D. Non-modified and Pt modified textile electrodes have shown their capacity to decolorize over 90 % the initial

amaranth solution in electroreduction and electrooxidation electrolysis, respectively. The presence of dispersed Pt in the WE2D and WE2D/PANI electrodes produced a remarkable reduction in the time of electrolysis. The UV and FTIR-ATR analysis provided evidence of the different behavior of the textile electrodes depending on their nature and the presence or absence of chloride ion in the amaranth solution.

5 Acknowledgments

The authors wish to acknowledge to the Spanish Ministerio de Ciencia e Innovación (contract CTM2011-23583) and Universitat Politècnica de València (Vicerrectorado de Investigación PAID-06-10 contract 003-233) for the financial support and to the company Carbongen S.A., Cocentaina, Spain, that kindly donated the activated carbon fabric. J. Molina is grateful to the Conselleria d'Educació, Formació i Ocupació (Generalitat Valenciana) for the Programa VALi+D Postdoctoral Fellowship. A.I. del Río is grateful to the Spanish Ministerio de Ciencia y Tecnología for the FPI fellowship.

6 Bibliography

- [1] Marsh H, Reinoso FR (2000) Sciences of carbon materials. Publicaciones de la Universidad de Alicante
- [2] Kinoshita K (1998) Carbon: electrochemical and physicochemical properties. Wiley, New York, pp 293-387
- [3] Burchell TD (1999) Carbon materials for advances technologies. Pergamon

- [4] Domínguez SD, Pardilla JA, Murcia AB, Morallón E, Amorós DC (2008) Electrochemical deposition of Pt nanoparticles on different carbon supports and conducting polymers. *J Appl Electrochem* 38:259-268
- [5] Kezhong W, Xu M, Xindong W, Jingling L (2005) Pt-Polyaniline-modified carbon fiber electrode for the electrooxidation of methanol. *Rare Metals* 24:33-36
- [6] Wu G, Li L, Li JH, Xu BQ (2006) Methanol electrooxidation on Pt particles dispersed into PANI/SWNT composite films. *J Power Sources* 155:118-127
- [7] Singh RN, Awasthi R, Tiwari SK (2010) Electro-catalytic activities of binary nano-composites of Pt and nano-carbon/multiwall carbon nanotube for methanol electro-oxidation. *Open Catal J* 3:50-57
- [8] Zhiani M, Rezaei B, Jalili J (2010) Methanol electro-electrooxidation on Pt/C modified by polyaniline nanofibers for DMFC applications. *Int J Hydrogen Energ* 35:9298-9305
- [9] Laborde H, Léger J-M, Lamy C (1994) Electrocatalytic electrooxidation of methanol and C1 molecules on highly dispersed electrodes. Part 1: Pt in polyaniline. *J Appl Electrochem* 24:219-226
- [10] Niu L, Li Q, Wei F, Wu S, Liu P, Cao X (2005) Electrocatalytic behaviour of Pt-modified polyaniline electrode for methanol electrooxidation: Effect of Pt deposition modes. *J Electroanal Chem* 578:331-337
- [11] Huang LM, Tang WR, Wen TCh (2007) Spatially electrodeposited Pt in polyaniline doped with poly(styrene sulfonic acid) for methanol electrooxidation. *J Power Sources* 164:519-526

- [12] Snehalatha M, Ravikumar C, Sekar N, Jayakumar SV, Joe H (2008) FT-Raman, IR and UV-visible spectral investigations and ab initio computations of a nonlinear food dye amaranth. *J Raman Spectrosc* 39:928-936
- [13] Rajendran L, Ananthi SP (2004) Analysis of positive feedback currents at the scanning electrochemical microscope. *J Electroanal Chem* 561:113-118
- [14] Niu L, Li Q, Wei F, Chen X, Wang W (2003) Formation optimization of Pt-modified polyaniline films for the electrocatalytic electrooxidation of methanol. *Synthetic Met* 139:271-276
- [15] Sala M, del Río AI, Molina J, Cases F, Gutierrez-Bouzán MC (2012) Influence of cell design and electrode materials on the decoloration of dyeing effluents. *Int J Electrochem Sc* 7:12470-12488
- [16] Priyantha N, Malavipathirana S (1996) Effect of chloride ions on the electrochemical behavior of platinum surfaces. *J Natn Sci Coun Sri Lanka* 24:237-246

Figure captions

Fig1 Voltammograms on WE2D of (a) Pt electrodeposition and (b) aniline electropolymerization at 10 mV s^{-1} and 5 mV s^{-1} , respectively. Voltammograms on WE1D of (c) Pt electrodeposition and (d) electropolymerization of aniline at 10 mV s^{-1} and 20 mV s^{-1} , respectively. (e) Voltammograms on WE1D/PANI of Pt electrodeposition at 10 mV s^{-1} scan rate

Fig2 (a) Approach curves in $0.01 \text{ M Ru(NH}_3)_6^{3+}$ and $0.1 \text{ M K}_2\text{SO}_4$ solution at pH 2.5 on: WE2D (×), WE2D/Pt (●), WE2D/PANI (+) and WE2D/PANI-Pt (⌘). (b) Approach curves at pH 5.5 on: WE2D (×), WE2D/PANI (+) and WE2D/PANI-Pt (⌘). The

theoretical feedback + curve has been included (—). The 100 μm diameter Pt SECM-tip was polarized at -300 mV vs Ag/AgCl and the approach rate was $10 \mu\text{m s}^{-1}$

Fig3 (a) Stereoscopic image of a WE2D modified with 20 Pt electrodeposition cycles. (b) SEM micrograph of the Pt dispersed particles. (c) SEM micrograph of PANI structures on carbon fibers synthesized after 5 CV cycles. (d) SEM micrograph of carbon fibers coated with PANI (5 CV cycles) and Pt particles (20 CV cycles). SEM micrographs were obtained at 3000x and 25000x magnification

Fig4 Cyclic voltammograms on WE1D for the (a) amaranth electroreduction (b) amaranth electrooxidation. (c) Cyclic voltammogram for amaranth on GG. All the voltammograms were recorded in a 600 mg L^{-1} amaranth and $0.5 \text{ M H}_2\text{SO}_4$ solution. Voltammograms in $0.5 \text{ M H}_2\text{SO}_4$ (dashed line) are also shown. Scan rate 10 mV s^{-1}

Fig5 % decolorization curves of the 60 mg L^{-1} amaranth and $0.5 \text{ M H}_2\text{SO}_4$ electroreduction versus (a) specific charge $Q (\text{A h L}^{-1})$ and (b) time of the electrolysis (h) on WE2D (at 0 mV, -500 mV and -800 mV), WE2D/Pt and WE2D/PANI-Pt (at 0 mV and -100 mV)

Fig6 % decolorization curves of the 60 mg L^{-1} amaranth and $0.5 \text{ M H}_2\text{SO}_4$ electrooxidation versus (a) specific charge $Q (\text{A h L}^{-1})$ and (b) time of the electrolysis (h) on WE2D, WE2D/Pt and WE2D/PANI-Pt at 900 mV in the presence/absence of chloride ion

Fig7 UV-visible spectra of the final samples from the electroreduction on (a) WE2D (at 0 mV, -500 mV and -800 mV) and WE2D/Pt, WE2D/PANI-Pt (at 0 mV and -100 mV) after 0.40 A h L⁻¹. The spectrum of the initial sample is also included

Fig8 UV-visible spectra of the final samples from the electrooxidation on WE2D, WE2D/Pt and WE2D/PANI-Pt at 900 mV in the presence/absence of chloride ion after 0.07 A h L⁻¹. The spectrum of the initial sample is also included

Fig9 FTIR-ATR spectra recorded for samples taken at the end of the electroreduction/electrooxidation electrolysis in the absence/presence of chloride ion. All spectra were recoded with a spectral slit width of 8 cm⁻¹

Table captions

Table1 Parameters of the carbon fabric used in the present work

<i>Parameters</i>	<i>Units</i>	<i>Values</i>
Weight	g/m ²	105 ± 5
BET ^a	m ² /g	1100 ± 100
Iodine index ^b	mg I ₂ /g	1100 ± 50
Permeability ^c	mm/s	728 ± 44
Thickness ^d	mm	0.505 ± 0.016
Tensile strength ^e <i>Warp</i>	N	230 ± 23
Tensile strength ^e <i>Weft</i>	N	120 ± 18
Elongation ^e <i>Warp</i>	%	4.60 ± 1.19
Elongation ^e <i>Weft</i>	%	8.28 ± 0.40
LOI ^f	%	48

^a BET: Brunauer, Emmet and Teller. Results got applying this statistical equation to N₂ isotherm adsorption at -196 °C. ^b ASTM D 4607-86 modified using photometric determination. ^c UNE EN ISO 9237:1999. ^d UNE EN ISO 5084:1997. ^e UNE EN ISO 13934-1:1999. ^f UNE EN ISO 4589-2:2001.

Figure1
[Click here to download high resolution image](#)

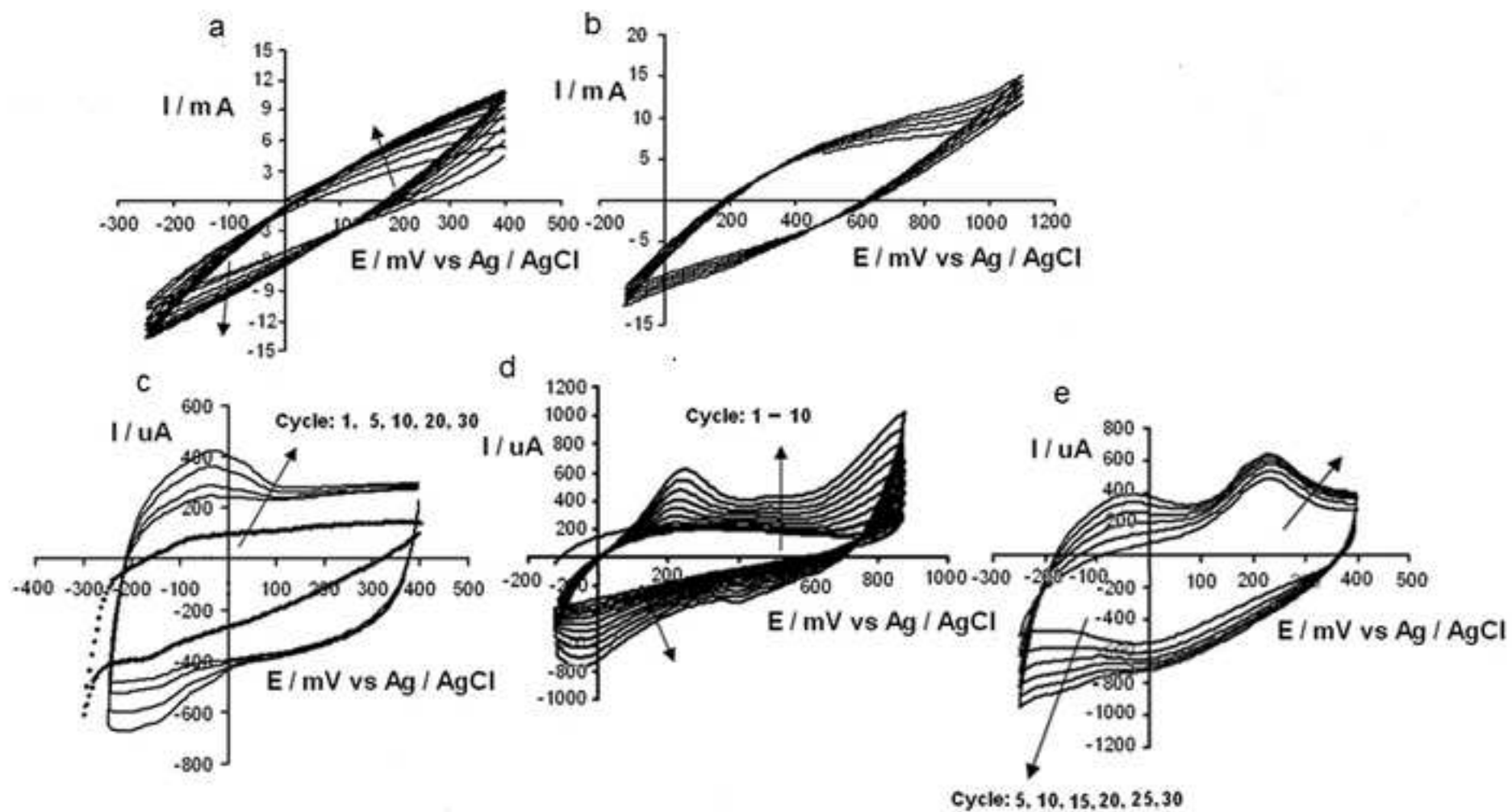


Figure2
[Click here to download high resolution image](#)

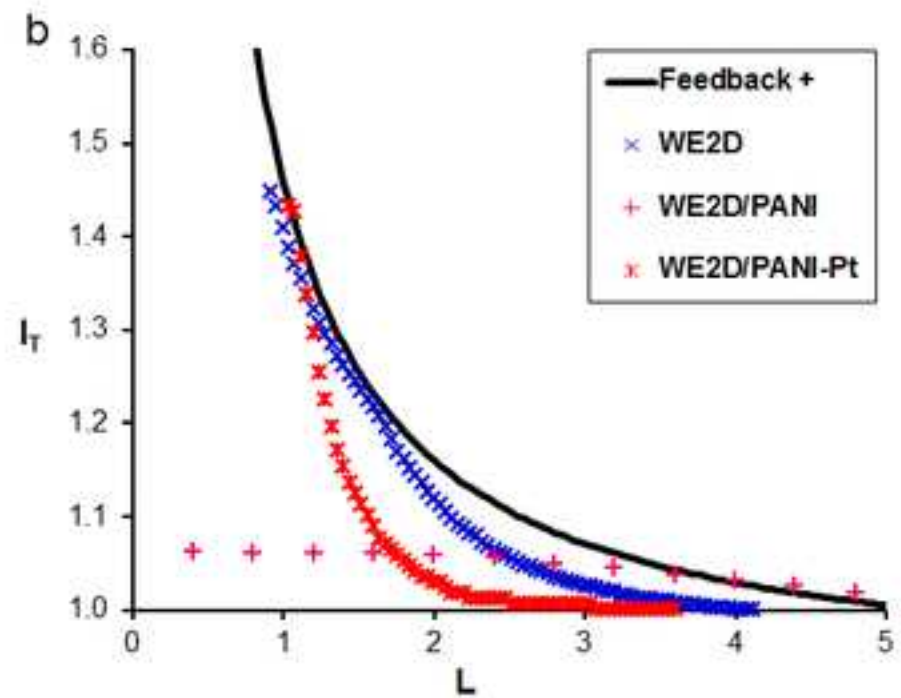
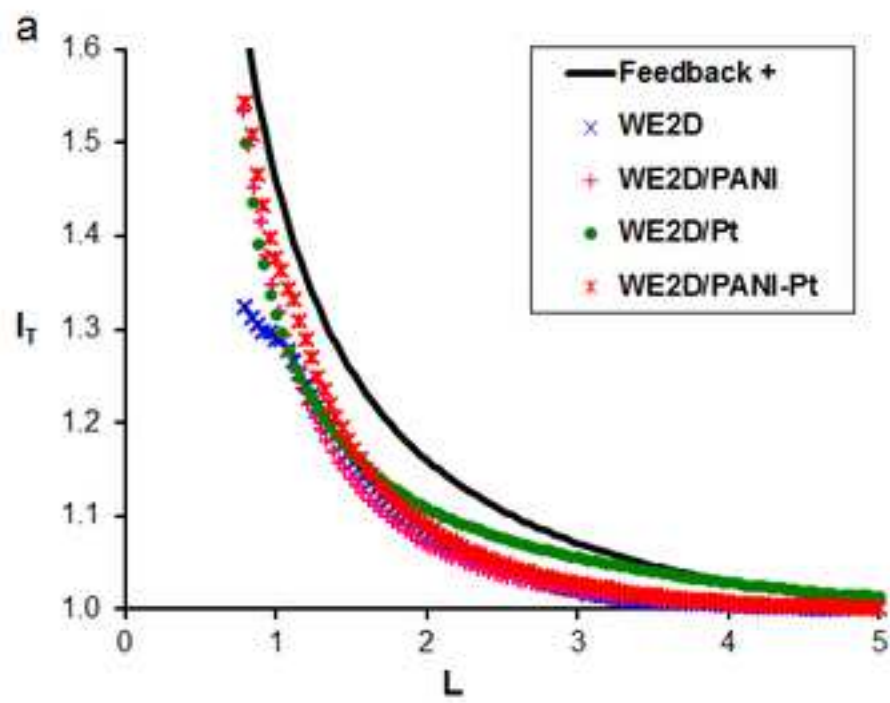


Figure3
[Click here to download high resolution image](#)

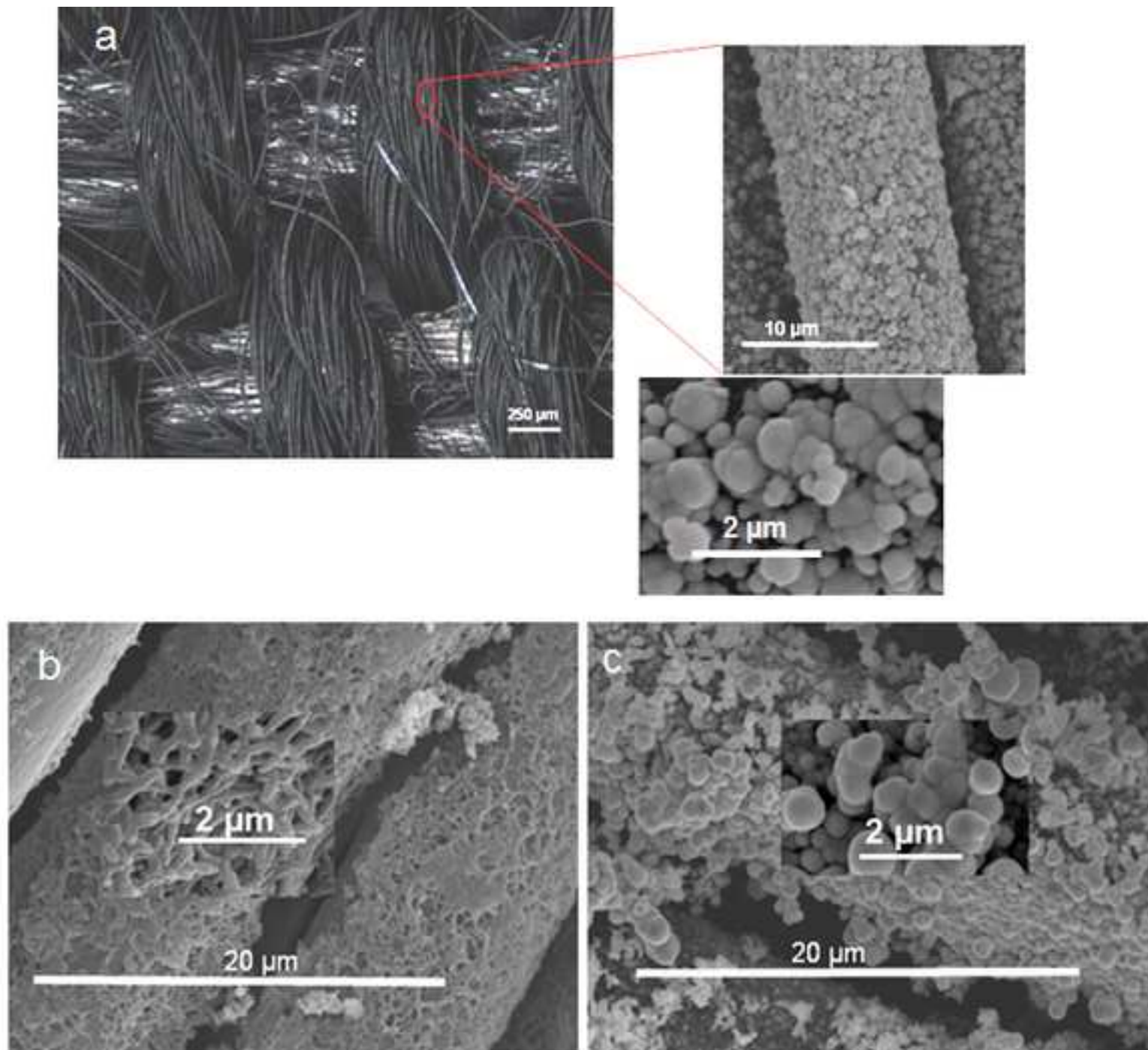


Figure4
[Click here to download high resolution image](#)

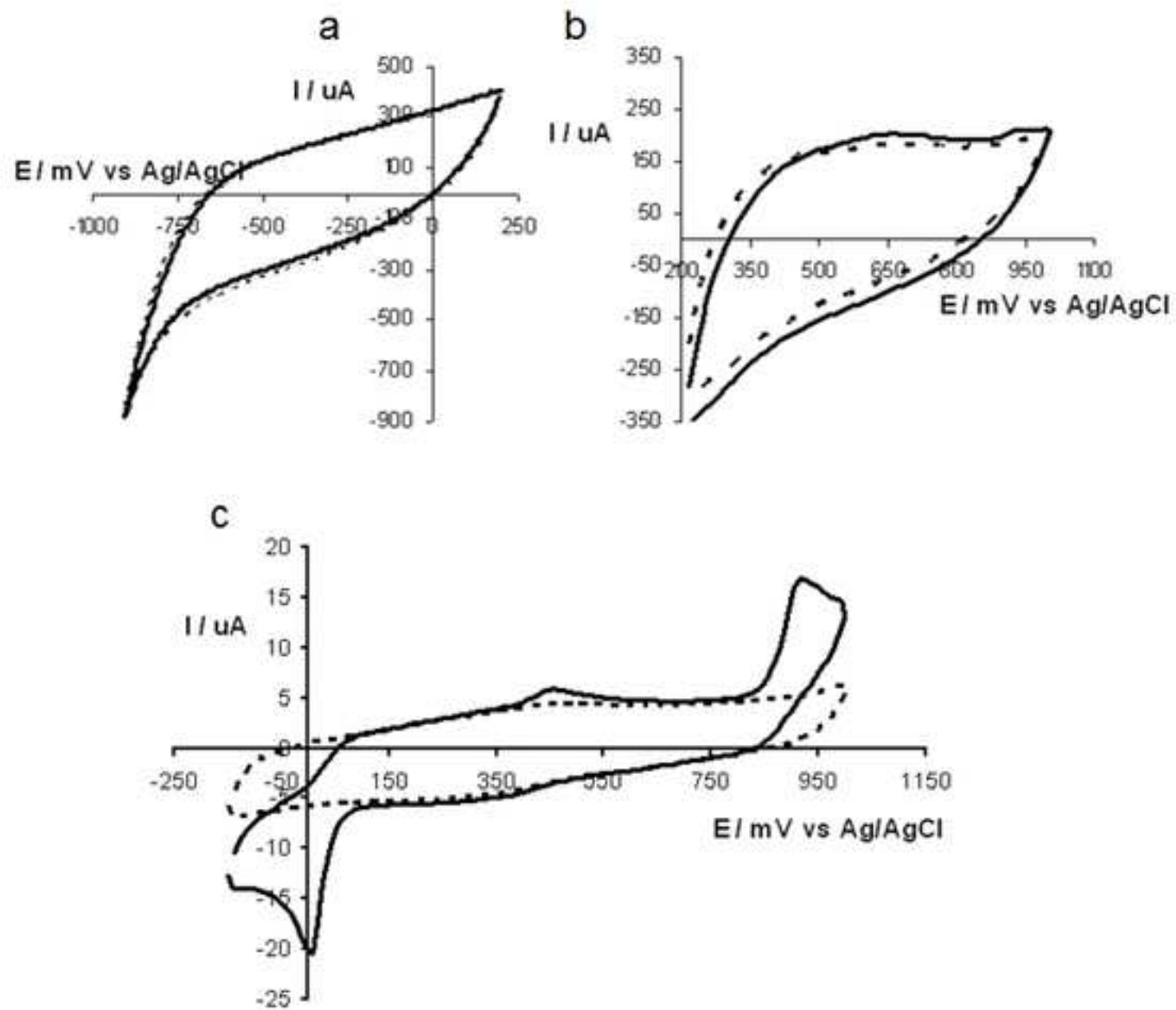


Figure 5

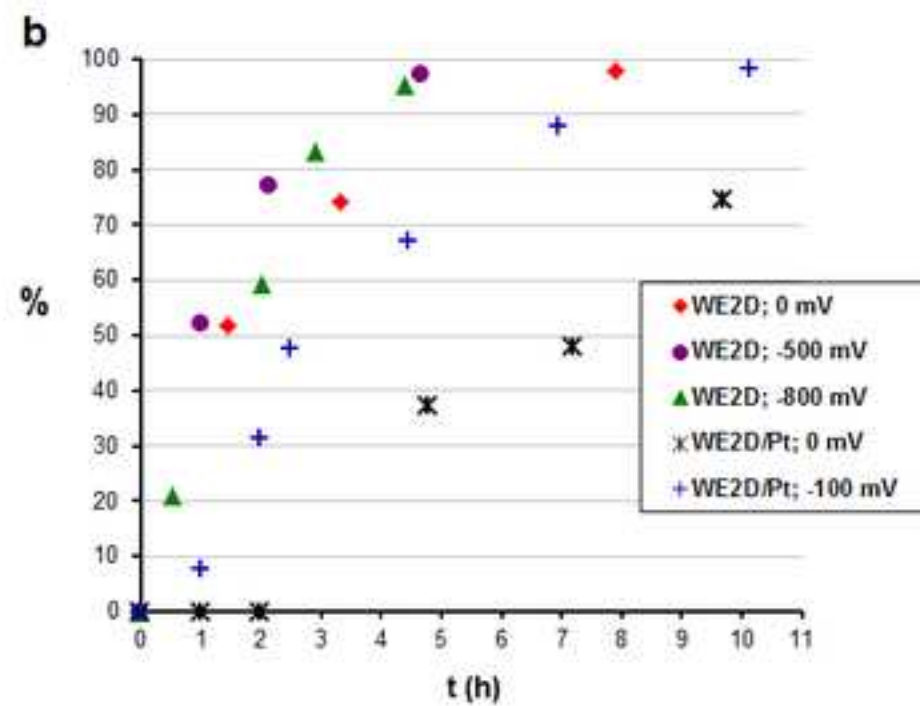
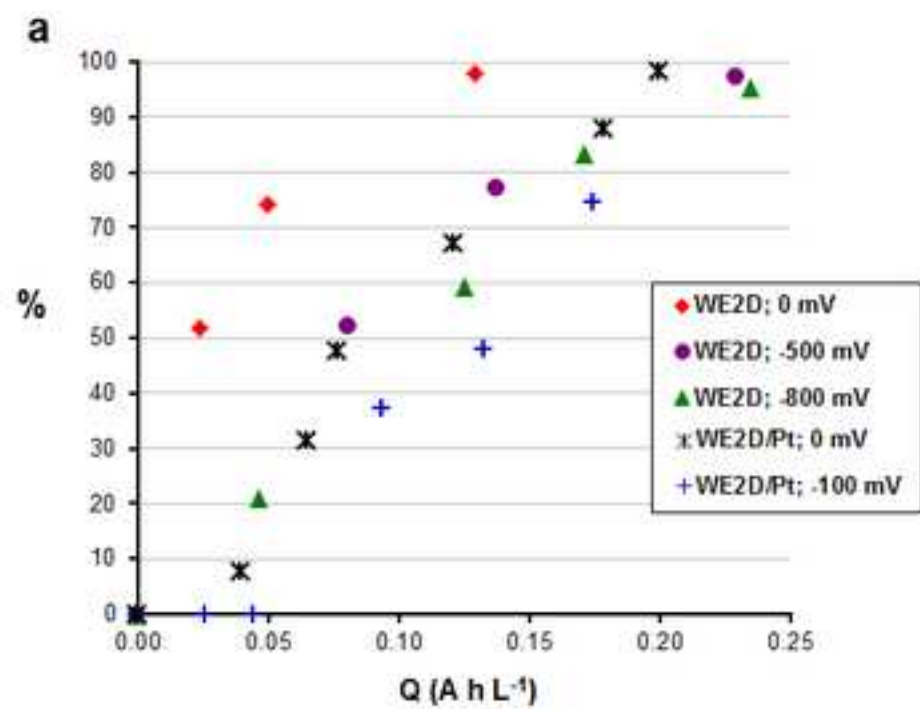
[Click here to download high resolution image](#)

Figure6
[Click here to download high resolution image](#)

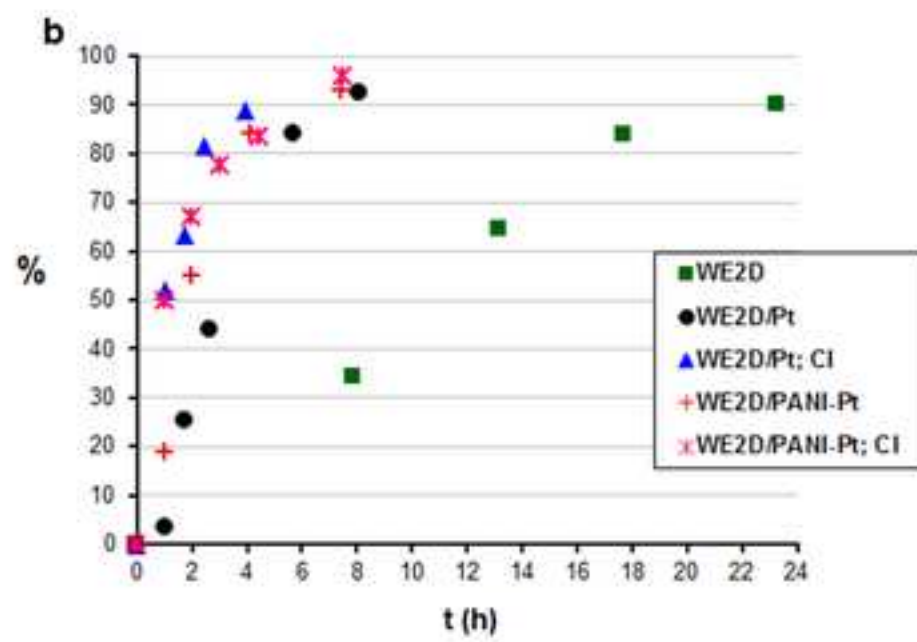
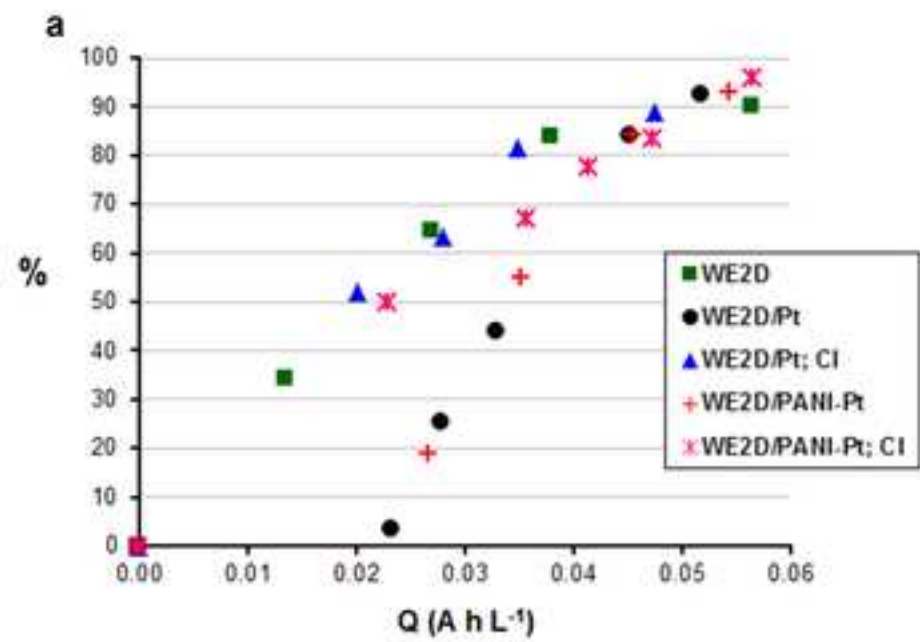


Figure 7

[Click here to download high resolution image](#)

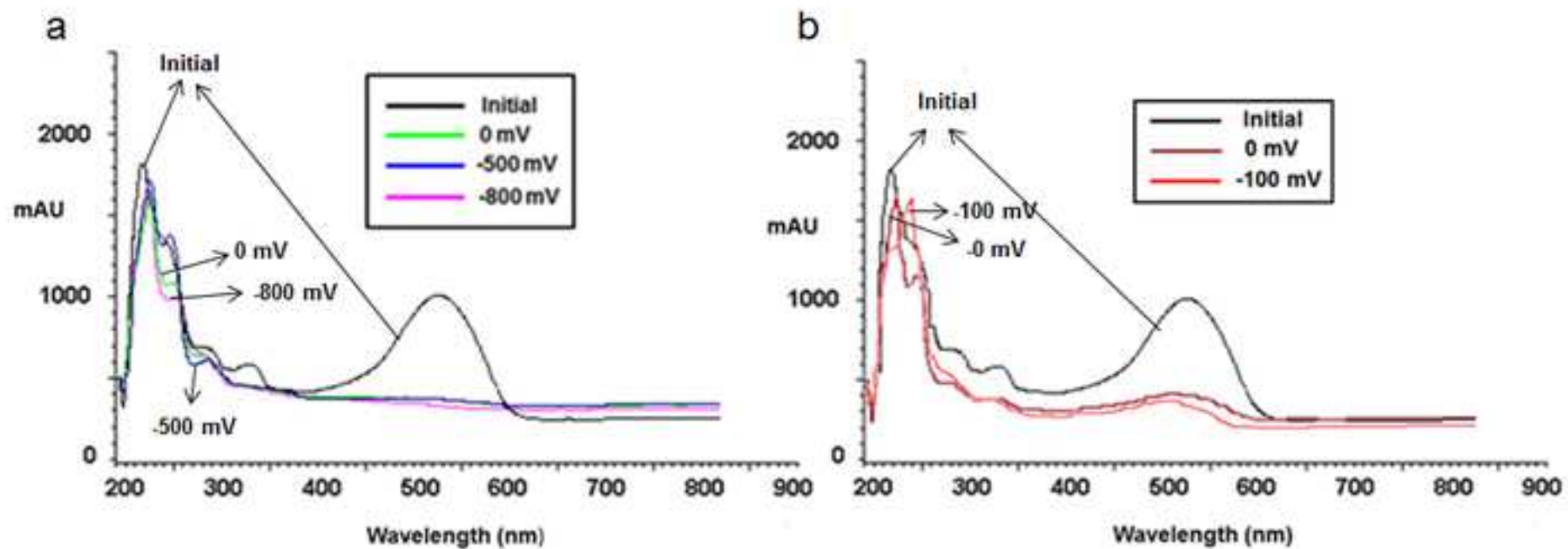


Figure8
[Click here to download high resolution image](#)

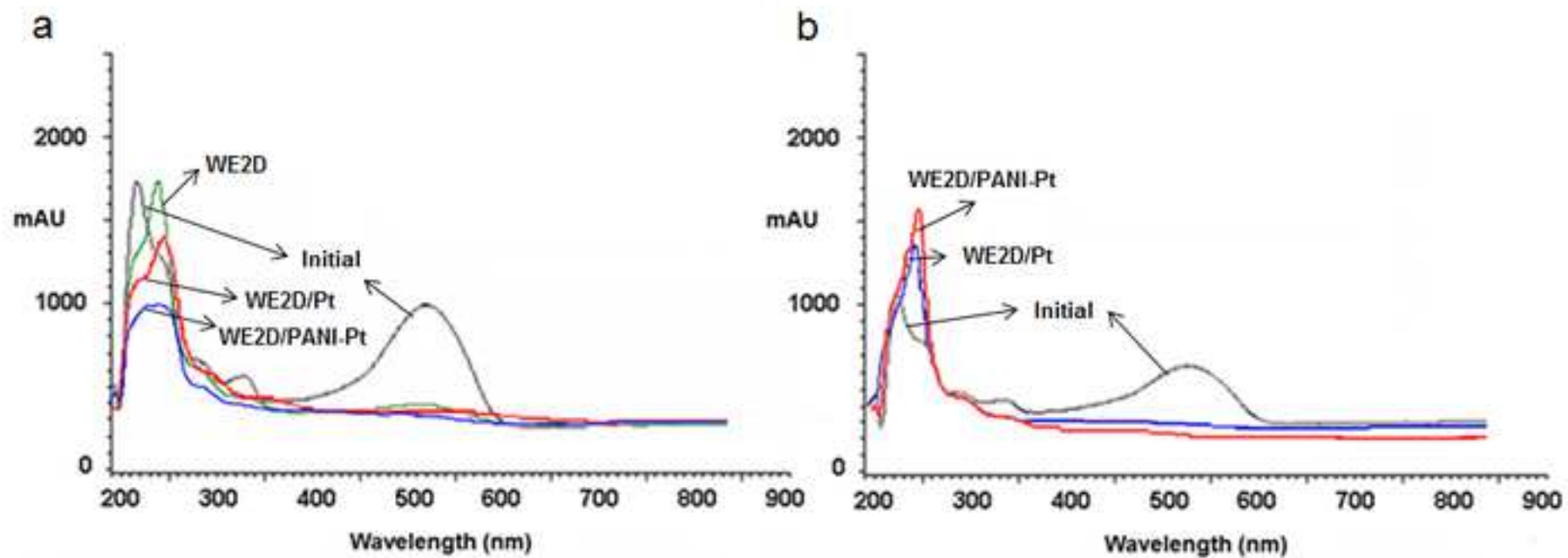


Figure9
[Click here to download high resolution image](#)

